THERMOMECHANICAL BEHAVIOUR OF SHORT GLASS FIBRE REINFORCED POLYAMIDE

A. Ayadi[a,b*], F. Roger[a], H. Nouri[a], H. Maitournam[c] and I. Raoult[d]

[a]*Mines Douai, Department of Polymers and Composites Technology & Mechanical Engineering, 941 rue Charles Bourseul, CS 10838, 59500 Douai, France*
[b]*Université de.Lille1, Nord de France*
[c]*Unité de Mécanique, ENSTA ParisTech , 91120 Palaiseau, France*
[d]*PSA Peugeot Citroën , Direction Scientifique et des Technologies futures, Route de Gisy, 78943 Vélizy-Villacoublay, cedex, France*

**Abderrahmane.ayadi@mines-douai.fr*

Keywords: Short glass fibre reinforced thermoplastics, thermomechanics, IR thermography, Fibre distribution, X-Ray tomography

Abstract
Short Glass Fibre Reinforced Polyamide 6.6 composites are increasingly used in structural automotive applications. The resulting fibre distribution within injection-moulded components has a major impact on their mechanical properties due to the complex flow path taking place while filling the mold. Even for simple structural geometries, resulting mechanical fields are heterogeneous. Moreover, the mechanical behavior of polyamide composites is sensitive to mechanical loads and especially to environmental conditions such as temperature and humidity.
In this work, we propose to use Infrared Thermography to monitor heterogeneous energy dissipation during tensile tests for different PA66GF35 specimens with various short glass fibre distributions. In addition, the thermoelasto-viscoplastic constitutive model developed by A.Launay was used to simulate temperature evolution during the tests. It is shown that particular attention must be paid to improve fibre distribution considerations for a right prediction of thermoelastic couplings.

1. Introduction

In the recent years, ecological production context has incited automotive industrials to increasingly use Short Glass Fibre Reinforced Polymers (SGFRP) for saving cars weight. Because of their mechanical performance and chemical resistance, polyamide-6.6 (PA66) composites are used as stressed functional automotive parts like intake manifolds, fuel injection rails, steering column switches, clutch pedal and oil pans [1]–[4]. SGFRP components with complex shapes are easily obtained by injection molding process. However, modeling their resulting mechanical properties has become more difficult. In fact, the reinforcing fibers dispersed in the melted matrix, are distributed according to the fluid dynamic processes taking place inside the mould. Even for simple geometries like thin plates this process leads to a layered skin-shell-core [5], [6] structure as depicted in **figure 1**.

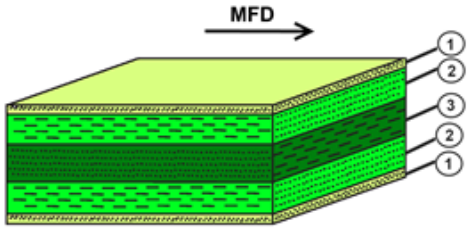

Figure 1. Representative scheme of a **s**kin (1)-shell (2)-core (3) structure
The arrow indicates the Mould Flow Direction (MFD)

During the mould filling, shear effects are induced by the velocity profile over the mould thickness. In the shell layers the fibres are mainly oriented parallel to mould flow direction (MFD) while in core layer they are generally orientated perpendicular to flow direction. In the external skin layers the melted material enters in contact with the cold mould walls resulting in random distribution. A number of methods are used to analyze fibre orientation within short glass fibre reinforced polymers such as: light microscopy, confocal laser scanning microscopy and Micro-Computed Tomography (µ-CT) [7]. The latter technique is used in our case to provide a 3D reconstruction of X-ray absorption within the sample.

To analyze the effect of fibre distribution on the mechanical behavior of SGFP, Infrared (IR) thermography was used to monitor temperature variations at the surface of the tested samples. An example of thermography-based quantitative analysis is the thermoelastic stress analysis (TSA), which is an experimental method of stress measurement based on the thermoelastic effect.
Thermal variations in anisotropic materials do occur not only for thermoelastic effect, but also for irreversible transformations[8][9].The thermoelastic effect, consists in the reversible temperature variation, occurring in a solid when it is deformed in the elastic field, and due to volume variation.

In this study, the plan of our work is as follows: in section 2, we will present thermomechanical equations that govern dissipation during the mechanical tests. To study the effect the heterogeneity of fibre distribution on the thermomechanical behavior different samples preparation will be described in section3. Moreover, the different used characterization techniques will be presented. Our results will be exposed in section 4.

2. Thermomechanical modeling

2.1. Launay's nonlinear anisotropic model

The thermomechanical response of PA66-GF35 is highly nonlinear. A. Launay proposed an elasto-viscoplastic constitutive behaviour to model the mechanical response under a wide loading and environmental conditions. This model is viscoelastic at low stresses levels and viscoplasticity is activated at high stress levels. Softening is considered using an internal variable β affecting the initial anisotropic elastic tensor. Indeed, the initial stiffness matrix is multiplied by a decreasing function of β. Material parameters of the model can be affected by temperature as well as relative humidity.
For sake of simplicity, only the uniaxial formulation of this model is described here, a more detailed description can be found in [10] [11]**.** The 1D rheological Launay model with material parameters is shown in **figure 2**.

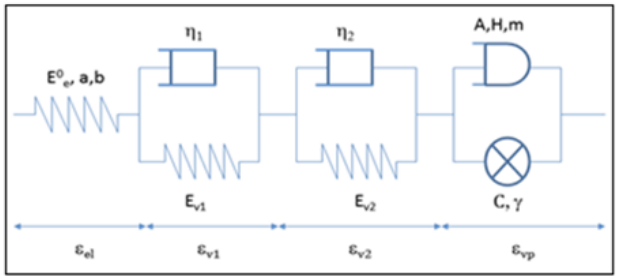

Figure 2. One-dimensional rheological representation of Launay's model

The total strain is partitioned into an elastic part ε_{el} with softening, a respectively long and short viscoelastic strains ε_{v1}, ε_{v2} and a viscoplastic strain ε_{vp}.

$$\varepsilon = \varepsilon_{el} + \varepsilon_{v1} + \varepsilon_{v2} + \varepsilon_{vp} \tag{1.1}$$

Only the viscoplastic evolution equation describing the evolution of plastic state variable as a function of the corresponding state variables is given:

$$\dot{\varepsilon}_{vp} = A\left[\sinh\left(\frac{\left|\sigma - \frac{3}{2}X\right|}{H}\right)\right]^m sign\left(\sigma - \frac{3}{2}X\right) \tag{1.2}$$

The back-stress tensor X is associated to hardening and corresponds to the center of the pseudo-viscoplastic surface. The dual corresponding hardening variable of X is α.

2.2. Thermomechanical couplings

Intrinsic dissipation can be written as the product of thermodynamical forces with corresponding fluxes.

$$D_{\text{int}} = A_{v1} : \dot{\varepsilon}_{v1} + A_{v2} : \dot{\varepsilon}_{v2} + A_{vp} : \dot{\varepsilon}_{vp} + X : \dot{\alpha} + A_{\beta}.\dot{\beta} \tag{1.3}$$

In the case, where we consider the following assumptions:
*the external heat supply or loss is time-independent
* the heat capacity C_{ε} is independent of internal state
* the heat convection term is neglected
the corresponding local heat equation during thermomechanical loading can then be written:

$$\rho C_{\varepsilon}\frac{\partial\theta}{\partial t} - \lambda\Delta\theta = D_{\text{int}} + \rho T\frac{\partial^2\psi}{\partial\varepsilon_{el}\partial T} : \dot{\varepsilon}_{el} \tag{1.4}$$

Where λ is the thermal conductivity, $\theta=T-T_0$ is the temperature variation. The last term in equation 1.4 corresponds to thermoplastic coupling. This equation, has been developed for thermoelastic conditions for orthotropic materials [12].
In the following section we will present the experimental configuration where the IR thermography will be conducted.

3. Material and experimental procedures

3.1. Material and samples

The totality of work was carried out on a 35 wt% short glass fibre reinforced polyamide (PA6.6). PA66GF35 is typically used for highly loaded plastic components in engine

compartments like intake manifolds, gears or fuel rails [3]. The trade name of the used grade is Zytel® 70G35 HSLX, a product of DuPontTM, kindly provided in the form of injection moulded 100 x 100 x 3 mm3 plates by PSA Peugeot Citroën, Velizy, France.
This material contains a fibre volume fraction of 19.5% and a number average aspect ratio of 25 (Fibres have a nominal diameter of 10 µm and an average fibre length, after injection moulding, of 250 µm). Conventional material data are compiled in **table 1**.

	Matrix (PA6.6)	E-glass fibre
Young Modulus (MPa)	1987	72,000
Poisson coef. (-)	0.4	0.22
Density (kg/m^3)	1.16	2.54

Table 1. Elastic properties of polyamide 6.6 matrix and glass fibre

The tested specimens were cut in the provided plates that were moulded through a divergent nap injection gate as shown in **figure 3**; at the entrance into the plate cavity the molten mass is forced to flow in a way that no good fibres alignment is obtained in center of the plate in flowing direction (axis e_1 in **figure 3**). The prediction of the average fibre orientation over the thickness according to the Moldflow simulation was done by *A.Launay et al*[10]. This simulation shows a high variability of fibre distribution even for simple geometries.

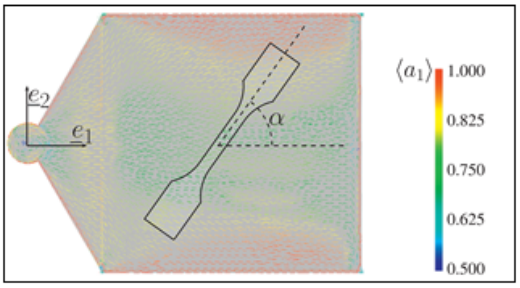

Figure 3. Average fibre orientation over the thickness as a result of an injection simulation of the plate with MOLDFLOW[10]

Different ISO527-2-5A samples were milled at three different orientations using an abrasive water jet. The chosen direction and the dimensions of the obtained specimens are depicted in **figures 4a** and **4b**.

In order to investigate the influence of the fiber orientation distribution on the thermo-mechanical response, three different orientations were chosen: the specimen orientation angle is defined as the angle between the Mould Flow Direction (MFD) and the specimen longitudinal axis. This angle is also referred as off-axis angle.

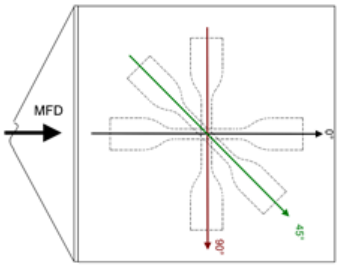

(a)

Figure 4. a Specimen orientation on the injection molded plate

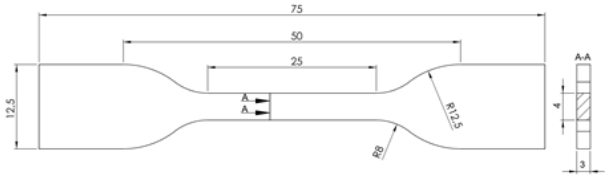

(b)

Figure 4.b ISO527-2-5A specimen geometry and **d**imensions [mm]

The samples were not subjected to any thermal conditioning. However the relative humidity of the matrix was identified close to 1.2 % using Karl Fisher analysis.

3.2. Tomography for fiber distribution analysis

An UltraTom X-Ray micro-tomography system was used in this study. X-ray images were collected by a 4000 × 2624 pixels CCD camera focused on a scintillating material using source energy of 160 keV. An in-plane pixel resolution of 800nm was attended.
The X-rays passing through the sample are absorbed according to spatial variations in composition and density, which provides the necessary contrast within the shadow image.
By rotating the sample at discrete angular increments of 0.25° and collecting a number of shadow images, individual cross-sections through the sample can be reconstructed. The reconstruction procedure was based on the back projection principle using Rx-Solutions commercial software X-Act.

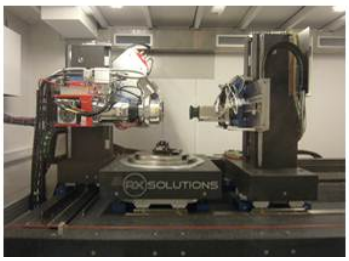

Figure 5. Ultra-Tom X-Ray tomography system

3.3. Mechanical testing

Monotonic tensile tests were carried out on an Instron 8501 hydraulic testing machine, recording the tensile strength and displacement. Tests were performed at room temperature (RT = 23°C). The machine was provided with a 100 kN load cell and a controlling software. Tests were carried out at crosshead rate of 2.5 MPa/s.

3.4. Combination of Infrared thermography and Digital Image Correlation investigation techniques

Infrared thermography was used to monitor real time temperature evolution during the mechanical tests. The Infrared camera used in this study is a CEDIP Jade III (Flir system) IR-thermal camera occupied with a G1-50mm objective and a 320 x 240 Focal Plane Array (FPA) sensor. The acquisition frequency was set up to 50Hz.
A previous thermal resolution calibration took place using an extended black body. For more measurement accuracy, the detection system takes into account the variation of the internal temperature of the camera.
The calibration setup was then introduced into the commercial software Altair (CEDIP Commercial Systems) to link each pixel's digital level of the FPA with the appropriate temperature.
In parallel, a high resolution camera was used to monitor the local displacement field evolution using digital image correlation. Vic 2D software was then used to analyze the corresponding strains fields.

It is expected that IR thermography and DIC used together can monitor the heterogeneity of mechanical field during tensile test on samples with heterogeneous fiber distributions.

4. Results and discussion

4.1. Micro-Computed Tomography

The obtained raw data were processed using a home developed protocol on the open source software ImageJ. Successive smoothing operations were applied followed by an automatic thresholding to each image of the volume stack was imposed. The resulting data were binarised then segmented with respect to the minimal accepted size of fibres corresponding to the nominal diameter.

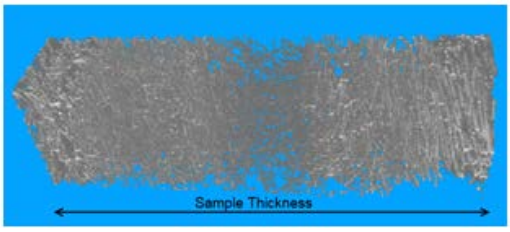

Figure 6. 3D reconstruction of the fibres within the PA66 matrix

As shown in figure 7, there is a skin-shell-core structure. The central zone is easily distinguished from the whole volume while random fibre distribution is observed in the shell layers.
Fiber distribution is summarized with orientation tensor in the 2D plane stress model of A.Launay. Tomography makes it possible to obtain the orientation tensor across the whole thickness.

4.2. Thermal evolution during tensile tests for various fibre distributions

Different specimens were cut in injected moulded plates at different angles (0°, 45° and 90°) as described in section 3.1. and were submitted to monotonic tensile test up to failure. Due to the specific orientation of each specimen in relation with the MFD, the local stiffness matrix field is heterogeneous. In the mold flow direction (0° angle) the fraction of fibres oriented in the loading direction is maximal; as a consequence the mechanical strength (ultimate stress) is higher. As the angle deviation from the MFD increases, the stiffness decreases. A directly injected specimen was added for comparison. In this last case, the stiffness is maximal. Infrared thermography monitors the temperature evolution and then the temperature increment in the whole specimen surface. After a thermoelastic stage where the temperature decreases, plasticity occurs and the local temperature variation becomes positive up to failure. The figures 8a and 8b show respectively the applied nominal stress-global strain evolution during monotonic tensile test and the corresponding temperature variation in the critical zone of the specimen which corresponds to the bottom of the specimen.
It is clearly seen that the higher the fraction of fibre is oriented in the loading direction, the higher is the ultimate stress. In the opposite, plasticity occurs early for transverse specimens where the fraction of MFD oriented fibres is weak and then the stiffness is weak. The strength of the injected specimen (figure 4b) is higher compared to the sample cut in the MFD in the plates.
This tends to show that material identification on directly injected specimens gives a poor estimation of the behavior of plates and complex mechanical components.

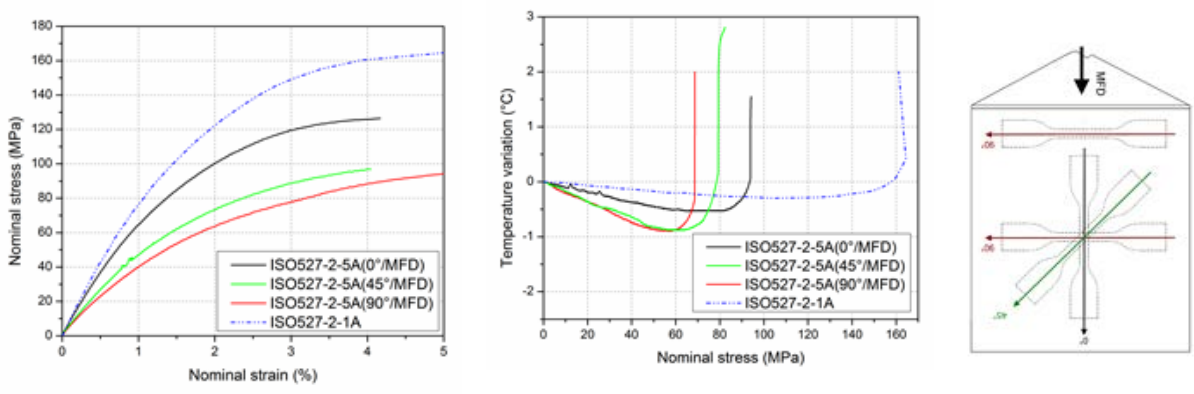

(a) (b) (c)

Figure 7. (a)Mechanical Response Of The Iso527-2-5a Samples Submitted To Monotonic Tensile Test (b)Temperature Variation During The Tensile Tests Response Of The Iso527-2-5a Samples (c)Samples Positions ; *****The Dashed Curves Correcpond To The Data Taken From [13] Relative To An Iso527-2-1a Specimen

4.3. Combination of infrared thermography and Digital Image Correlation to monitor heterogeneous thermomechanical fields

IR thermography gives temperature variation at the surface. We have seen (section 2) that temperature variation is correlated to stress state. D.I.C. estimates the surface strain field during the tensile test. It is expected that both techniques are reliable to monitor thermomechanical field heterogeneity.

We consider a tensile test specimen cut transversally to the MFD close to the injection gate as illustrated in **figure 7c** (top sample). Temperature variation in its critical zone is plotted in **figure 8a**. **Figures 8a1**, **8b1** and **8c1** show the temperature variation at three specific loading times respectively at the thermoelastic stage, at the end of the thermoelastic stage and before failure. It is seen that even during the thermoelastic stage, the critical zone can be identified. This shows that the critical zone is related to the heterogeneous stiffness in this area.

The same conclusion can be drawn with D.I.C. with strain field analysis in loading direction (**figures 8a2**, **8b3** and **8b4**) and transverse direction (**figures 8a3**, **8b3** and **8c3**).

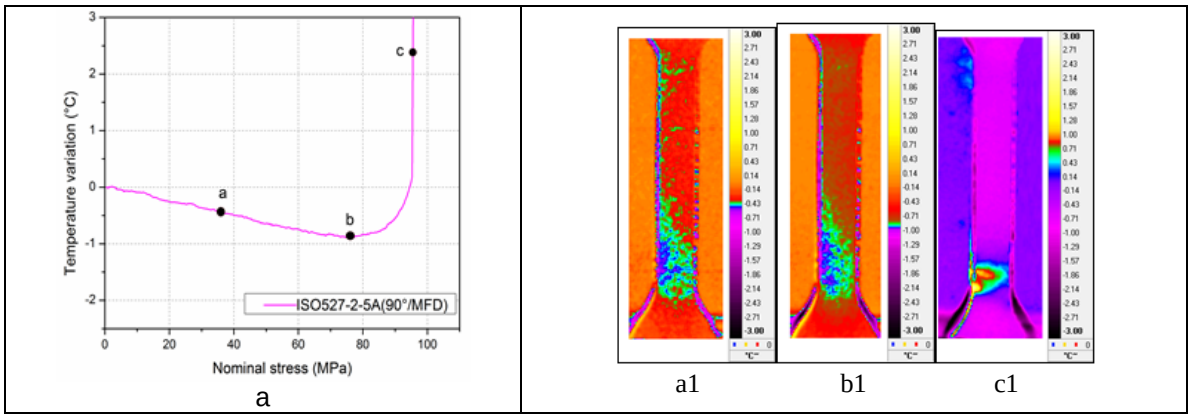

a

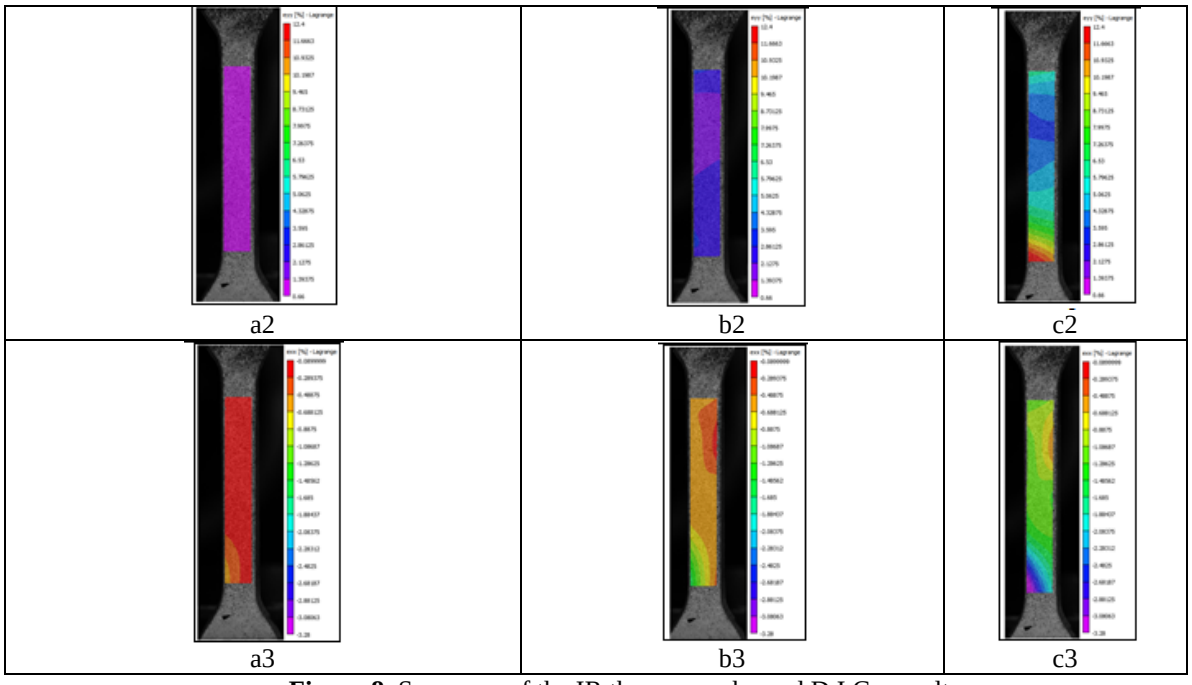

Figure 8. Summary of the IR thermography and D.I.C. results

References

[1] A. Bernasconi, P. Davoli, and C. Armanni, "Fatigue strength of a clutch pedal made of reprocessed short glass fibre reinforced polyamide," *Int. J. Fatigue*, 2010.

[2] V. Crupi and E. Guglielmino, "Application of Digital Image Correlation for the effect of glass fibres on the strength and strain to failure of polyamide plastics," *CONVEGNO IGF XXII …*, pp. 1–3, 2013.

[3] C. Sonsino and E. Moosbrugger, "Fatigue design of highly loaded short-glass-fibre reinforced polyamide parts in engine compartments," *Int. J. Fatigue*, vol. 30, no. 7, pp. 1279–1288, Jul. 2008.

[4] Z. Mouti, K. Westwood, D. Long, and J. Njuguna, "An experimental investigation into localised low-velocity impact loading on glass fibre-reinforced polyamide automotive product," *Compos. Struct.*, vol. 104, pp. 43–53, Oct. 2013.

[5] M. F. Arif, N. Saintier, F. Meraghni, J. Fitoussi, Y. Chemisky, and G. Robert, "Multiscale fatigue damage characterization in short glass fiber reinforced polyamide-66," *Compos. Part B Eng.*, vol. 61, pp. 55–65, May 2014.

[6] M. De Monte, E. Moosbrugger, and M. Quaresimin, "Influence of temperature and thickness on the off-axis behaviour of short glass fibre reinforced polyamide 6.6–Quasi-static loading," *Compos. Part A Appl. …*, 2010.

[7] C. N. Eberhardt and a R. Clarke, "Automated reconstruction of curvilinear fibres from 3D datasets acquired by X-ray microtomography," *J. Microsc.*, vol. 206, no. Pt 1, pp. 41–53, Apr. 2002.

[8] L. Vergani, "A review of thermographic techniques for damage investigation in composites," *Frat. e Integrita …*, vol. 27, pp. 1–12, 2014.

[9] a. Ghorbel, N. Saintier, and a. Dhiab, "Investigation of damage evolution in short glass fibers reinforced polyamide 6,6 under tensile loading using infrared thermography," *Procedia Eng.*, vol. 10, pp. 2123–2128, Jan. 2011.

[10] a. Launay, M. H. Maitournam, Y. Marco, and I. Raoult, "Multiaxial fatigue models for short glass fiber reinforced polyamide – Part I: Nonlinear anisotropic constitutive behavior for cyclic response," *Int. J. Fatigue*, vol. 47, pp. 382–389, Feb. 2013.

[11] Y. Marco, V. Le Saux, L. Jégou, a. Launay, L. Serrano, I. Raoult, and S. Calloch, "Dissipation analysis in SFRP structural samples: Thermomechanical analysis and comparison to numerical simulations," *Int. J. Fatigue*, Feb. 2014.

[12] R. Haj-Ali, B.-S. Wei, S. Johnson, and R. El-Hajjar, "Thermoelastic and infrared-thermography methods for surface strains in cracked orthotropic composite materials," *Eng. Fract. Mech.*, vol. 75, no. 1, pp. 58–75, Jan. 2008.